Pressure fields in the vicinity of brass musical instrument bells measured using a two dimensional grid array and comparison with multimodal models

Kemp, J. A., Lopez-Carromero, A., & Campbell, M

24th INTERNATIONAL CONGRESS ON SOUND AND VIBRATION
23–27 July 2017, London

ICSV24
23-27JULY 2017
LONDON CALLING

PRESSURE FIELDS IN THE VICINITY OF BRASS MUSICAL INSTRUMENT BELLS MEASURED USING A TWO DIMENSIONAL GRID ARRAY AND COMPARISON WITH MULTIMODAL MODELS

Jonathan Kemp
University of St Andrews, Music Centre, St Andrews, UK
email: jk50@st-andrews.ac.uk

Amaya Lopez-Carromero
University of Edinburgh, School of Physics, Edinburgh, UK

Murray Campbell
University of Edinburgh, School of Physics, Edinburgh, UK

Brass musical instruments act as a source of spherical waves for low frequencies while at higher frequencies the directivity produces a diffracting beam. The directivity and radius of the wavefronts (and therefore the source position) may be expected to depend on the frequency in addition to the geometry of the bell. In this work, experimental determination of the wavefronts propagating from the bell section of brass instruments was performed using a moveable line array of microphones. Exponential sine sweep measurements were performed for each microphone position, effectively giving synchronised impulse responses at every microphone position in a two-dimensional grid starting directly in front of the bell. Calculations were then carried out to check to what extent the observed field was consistent with the predictions from multimodal theory. The multimodal radiation impedance was only known previously for specific geometries such as the infinite baffle, but here an extension of the theory is set out in order to simulate a trombone radiating within a large radius, infinite length cylindrical pipe.

Keywords: brass radiation multimodal microphone array

1. Introduction

Modal decomposition in a brass musical instrument bore can be achieved assuming a piecewise, axi-symmetric cylindrical model[1, 2, 3]. Previously this has involved the assumption that the instrument is terminated into an infinite baffle. In this work the method is extended to allow for the instrument to be set in an infinite cylindrical pipe, allowing energy to radiate both directly away from the bell and diffracting around the instrument to radiate to the other side of the instrument bell.

2. Multimodal decomposition with hard walled cylinders

The discretisation of the bore into piecewise cylinders placed axi-symetrically along the z axis involves hard walled discontinuities as shown in Figure 1. It is assumed that the axial distance between the surfaces $S^{(1)}$ and $S^{(2)}$ is infinitesimal. The complex pressure amplitude in three dimensions

(assuming cylindrical symmetry) is defined as [1]:

$$p(r,z,t) = \sum_{n=0}^{\infty} \mathbf{P}_n(z)\psi_n(r)\exp(j\omega t), \quad \psi_n(r) = \frac{J_0(\gamma_n r/R)}{J_0(\gamma_n)}, \tag{1}$$

where the infinite series must be truncated to a finite number for practical computation with the values of γ_n being the successive zeros of the Bessel function of the first kind of order one, r is the radius from the central axis and the hard wall on the outside of the cylinder is at $r = R$.

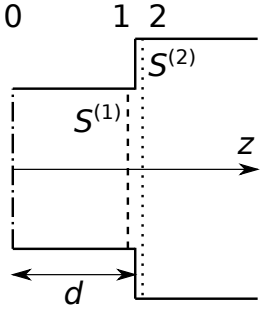

Figure 1: A cylinder of length d and cross-sectional area $S^{(1)} = \pi\left(R^{(1)}\right)^2$ opens out into a cylindrical pipe of cross-sectional area $S^{(2)} = \pi\left(R^{(2)}\right)^2$.

Matching pressure on $S^{(1)}$ (and leaving the pressure vector free on $S^{(2)} - S^{(1)}$) gives the condition for projection of the pressure amplitude vector for the transverse modes, $\mathbf{P}$, as [1]:

$$\mathbf{P}^{(1)} = F\mathbf{P}^{(2)}, \quad F_{n,m} = \frac{2x\gamma_m J_1(x\gamma_m)}{(x^2\gamma_m^2 - \gamma_n^2)J_0(\gamma_m)}, \tag{2}$$

and $F_{0,0} = 1$ and where $x = R^{(1)}/R^{(2)}$.

The vector of axial velocity amplitudes for the transverse modes (multiplied by the cross sectional area), U, projects across this discontinuity in accordance to the equation:

$$\mathbf{U}^{(2)} = F^{\top}\mathbf{U}^{(1)}, \tag{3}$$

where $F^{\top}$ is the transpose of F. As discussed by Pagneux et al [1], this condition corresponds to matching the acoustic particle velocity on $S^{(1)}$ while setting the acoustic particle velocity to zero on the hard wall ($S^{(2)} - S^{(1)}$). The procedure for projecting the impedance matrix and pressure and velocity vectors starting from a known radiation impedance and from the assumption of planar velocity at the source is discussed in detail in Pagneux et al [1], Amir et al [2] and Kemp [3] so will not be reviewed here explicitly. It should be noted that projection of the impedance matrix through a cylinder from surface 1 to surface 0 should be explicitly stated, however as this is a correction to the formulae from Pagneux et al [1] and from the original print of Kemp's thesis [3]. This projection formula for the geometry in Figure 1 is:

$$Z^{(0)} = A - B(Z^{(1)} + A)^{-1}B, \tag{4}$$

where A and B are diagonal matrices with the diagonal entries given by

$$A(n,n) = \frac{-j}{\tan(k_n d)}\frac{\rho c}{S^{(1)}}\frac{k}{k_n} \quad \text{and} \quad B(n,n) = \frac{-j}{\sin(k_n d)}\frac{\rho c}{S^{(1)}}\frac{k}{k_n} \tag{5}$$

where, assuming lossless propagation,

$$k_n = \sqrt{k^2 - (\gamma_n/R)^2}, \tag{6}$$

with k being the wavenumber. Lossy propagation may be simulated using k_n from [4, 2, 3]:

$$k_n = \pm\sqrt{k^2 - \left(\frac{\gamma_n}{R}\right)^2 + \left(\frac{2k}{R}\right)[\Im(\epsilon_n) - i\Re(\epsilon_n)]}, \tag{7}$$

where $\Re$ and $\Im$ mean taking the real and imaginary parts respectively, with

$$\epsilon_n = \left(1 - \gamma_n^2/(k^2R^2)\right)\epsilon_v + \epsilon_t, \quad \epsilon_v = (1+i)\,2.03\times10^{-5}f^{1/2}, \quad \epsilon_t = (1+i)\,0.95\times10^{-5}f^{1/2}, \tag{8}$$

where f is the frequency.

3. Monopole and dipole boundary conditions

Conditions for radiation from a membrane and disks in free space [5, 6, 7] are known. These cases feature a dipole type radiation as the front and back surfaces radiate in antiphase, as seen in Figure 2(a) giving a zero pressure condition at $z = 0$ beyond the edge of the source. The sound radiated from the source in an infinite baffle, as seen in Figure 2(b) will, in contrast, have zero for the axial component for the acoustic particle velocity on $z = 0$ beyond the edge of the source. Averaging the pressure radiated from a source on a baffle (monopole radiation) and a dipole radiating in free space yield the response of a one sided source radiating in free space as illustrated in Figure 2(c).

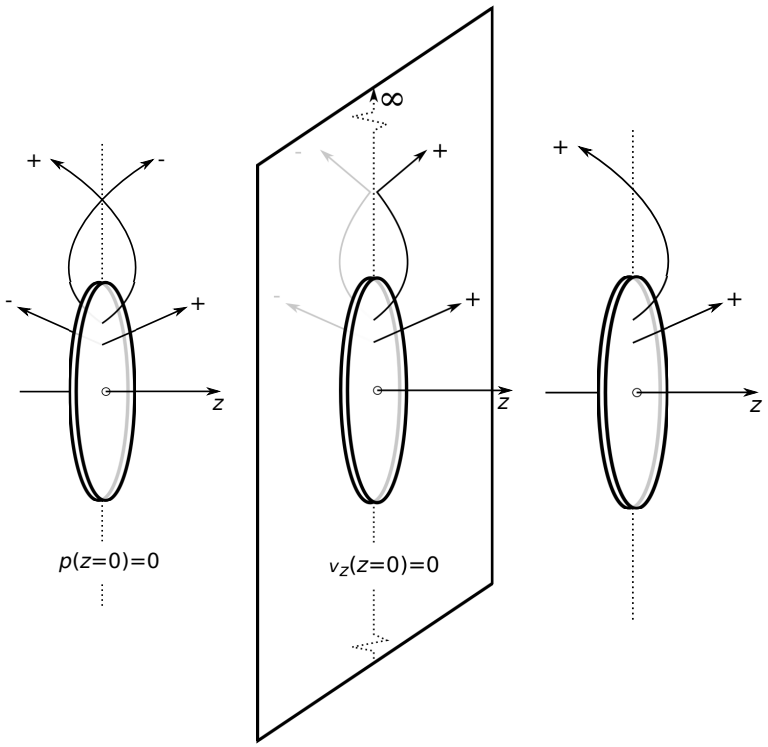

Figure 2: Dipole source with no baffle (a), source in an infinite baffle (b) and one sided source with no baffle (c). The pressure field for (c) in the range $z > 0$ should be the average of the pressure fields for cases (a) and (b). Each radiating surface has an arrow to schematise the phase of travelling pressure wave that radiates directly away from $z = 0$ and another arrow to schematise the phase of the travelling pressure wave that diffracts around to impact $z = 0$.

4. Multimodal decomposition approximating radiation into a cylinder extending to positive and negative infinity

Consider the case of an acoustic horn terminated in an (unbaffled) open end of cross-section $S^{(R)}$ that is itself enclosed in an external cylinder of infinite length with a cross-sectional area $S^{(E)}$ as shown in Figure 3.

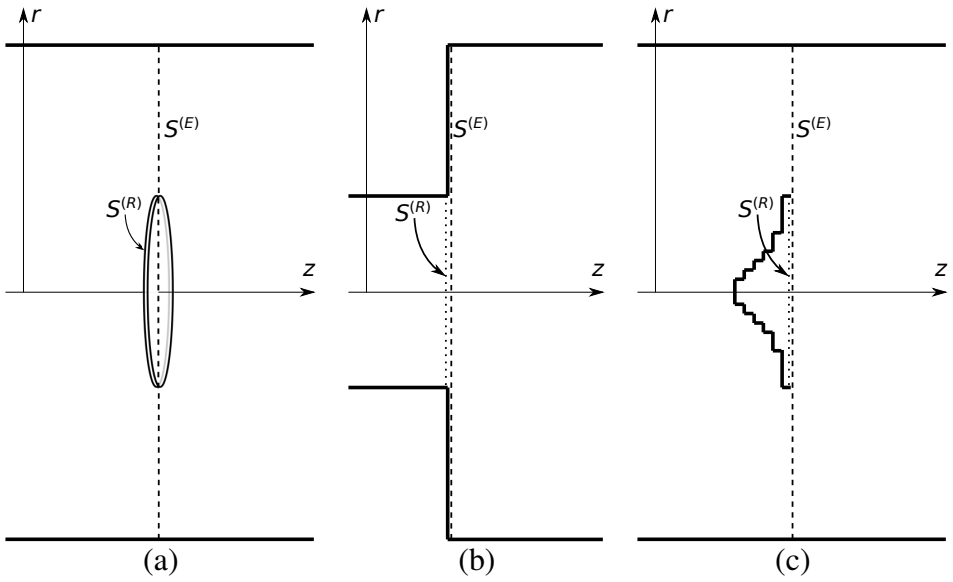

Figure 3: A two sided dipole source of surface area $S^{(R)}$ in a cylindrical pipe of surface area $S^{(E)}$ is shown in (a). A hard wall expansion from surface area $S^{(R)}$ to surface area $S^{(E)}$ is shown in (b). An acoustic horn approximated using piece-wise cylinders ending with a radiating cross-sectional area of $S^{(R)}$, opening out into an external cylindrical pipe of infinite length and of cross-sectional area $S^{(E)}$ is shown in (c).

Clearly, the radiation occurs in a manner similar to the one sided, unbaffled source of figure 2(c), but in this case we must include the effect of the external cylinder giving a set of modes on the cross-section $S^{(E)}$. In analogy to the discussion in section 3, the impedance matrix on the surface $S^{(R)}$ will be taken as being the average of the impedance matrix which would be observed for a zero axial velocity condition on $S^{(E)} - S^{(R)}$ and of the impedance matrix which would be observed for a zero pressure condition on $S^{(E)} - S^{(R)}$. In the case of the external pipe being infinite, the impedance $Z^{(E)}$ (on surface $S^{(E)}$) is known to be given by the (diagonal) characteristic impedance matrix [1], so $Z^{(E)} = Z_c$ where $Z_c(n,n) = \rho ck/(S^{(1)}k_n)$.

Projection to $S^{(R)}$ for the case of a hard wall (axial velocity zero on $S^{(E)} - S^{(R)}$) is well known to be given as [1]:

$$Z_h^{(R)} = F Z^{(E)} F^\top, \tag{9}$$

where it is assumed that the axial distance between the surfaces $S^{(R)}$ and $S^{(E)}$ is infinitesimal and where the subscript h indicates that the hard wall condition is being used for the surface $S^{(E)} - S^{(R)}$.

Projection to $S^{(R)}$ for the zero pressure condition on $S^{(E)} - S^{(R)}$ is given here as (equating axial velocity on $S^{(1)}$ and leaving the vector free on $S^{(2)} - S^{(1)}$):

$$\mathbf{U}_d^{(R)} = \left(S^{(R)}/S^{(E)}\right) F \mathbf{U}_d^{(E)}, \tag{10}$$

where the subscript d indicates that the dipole type radiation field is being used for the surface $S^{(R)}$ with no wall present on the surface $S^{(E)} - S^{(R)}$. Similarly, equating the pressures on $S^{(1)}$ and setting the pressure to zero on $S^{(2)} - S^{(1)}$ gives the vector of modal pressure amplitudes for the dipole type boundary condition as:

$$\mathbf{P}_d^{(E)} = \left(S^{(R)}/S^{(E)}\right) F^\top \mathbf{P}_d^{(R)}. \tag{11}$$

Defining the admittance matrix, $Y = Z^{-1}$ such that $\mathbf{U} = Y\mathbf{P}$, this then leads to the formula for admitance matrix projection:

$$Y_d^{(R)} = \left(S^{(R)}/S^{(E)}\right)^2 F Y^{(E)} F^\top. \tag{12}$$

The impedance for the dipole type field is then calculated by matrix inversion:

$$Z_d^{(R)} = \left(Y_d^{(R)}\right)^{-1}. \tag{13}$$

The impedance for the single sided radiator without baffle but in the external cylinder is then:

$$Z^{(R)} = \frac{1}{2}\left(Z_h^{(R)} + Z_d^{(R)}\right). \tag{14}$$

It should be noted that fewer modes should be used on the negative z side of the large discontinuity (within the bore) so, in practice, truncation of $Y_d^{(R)}$ before applying Equation 13 and, similarly, truncation of $Z_h^{(R)}$ in Equation 14 is required to achieve good accuracy as discussed in section 4.1.

Projecting the pressure vector from $S^{(R)}$ to $S^{(E)}$ assuming a one sided radiation condition involves averaging the pressure calculated for the dipole condition, $\mathbf{P}_d^{(E)}$ from Equation 11, and the pressure for the hard wall condition,

$$\mathbf{P}_h^{(E)} = F\mathbf{P}_h^{(R)} \tag{15}$$

from Equation 2:

$$\mathbf{P}^{(E)} = \frac{1}{2}\left(\mathbf{P}_d^{(E)} + \mathbf{P}_h^{(E)}\right), \tag{16}$$

and the volume velocity on the surface $S^{(E)}$ is given by:

$$\mathbf{U}^{(E)} = \left(Z^{(E)}\right)^{-1}\mathbf{P}^{(E)}. \tag{17}$$

4.1 Numerical procedure for pressure field calculations

The radius against axial distance for the internal bore of brass instruments was tabulated making use of direct calliper measurements where possible. A piecewise cylindrical model of the internal instrument bore (to the negative z side of the surface $S^{(R)}$), and a section of the external cylindrical bore (to the positive z side of the instrument bell's radiating surface $S^{(R)}$), was then created in MATLAB. The multimodal impedance matrix and pressure field were calculated using the following process:

- The (multimodal) impedance matrix (for a chosen frequency of interest) was set to be equal to the characteristic impedance matrix for all axial points on the external cylinder with the number of modes included in the calculation within the external cylinder labelled $N^{(E)}$.
- Equations 12 and 9 were used to calculate $Y_d^{(R)}$ and $Z_h^{(R)}$ respectively from $Z^{(E)} = Z_c$. These matrices were then truncated to size $N^{(R)} \times N^{(R)}$ to ensure good accuracy.
- The impedance $Z^{(R)}$ (on the surface $S^{(R)}$) was obtained using Equation 14 (which in turn requires the use of Equations 13).
- The impedance matrix was projected alternately using Equation 4 (for projection down a cylinder) and $Z^{(1)} = FZ^{(2)}F^\top$ (for projection across a discontinuity) until the input of the brass instrument was reached. The impedance matrix was stored at all steps along the bore.
- A planar source is assumed at the input so $\mathbf{U}^{(0)} = [1, 0, 0, 0, 0, 0, 0, ...]^\top$ with size $N^{(R)} \times 1$.
- Following this, the vectors were alternately projected along the cylinder to give $\mathbf{U}^{(1)}$ (as described in Equation 25 of Pagneux et al [1]) and then projected across the discontinuity to obtain $\mathbf{U}^{(2)}$ using Equation 3 until the radiating surface $S^{(R)}$ is reached, storing $\mathbf{P} = Z\mathbf{U}$ at each point along the bore.
- The vectors $\mathbf{P}^{(R)}$ and $\mathbf{U}^{(R)}$ are then zero padded to increase their size from $N^{(R)} \times 1$ to $N^{(E)} \times 1$.
- The vector $\mathbf{P}^{(R)}$ is projected to give $\mathbf{P}^{(E)}$ using Equation 16 (which in turn requires using Equations 11 and 15 with $\mathbf{P}_d^{(R)} = \mathbf{P}_h^{(R)} = \mathbf{P}^{(R)}$).

- $\mathbf{U}^{(E)}$ is obtained from Equation 17.
- The vector of axial velocities for the modes, $\mathbf{U}$, is then projected along the external cylinder in discrete points along the z axis using Equation 25 of Pagneux et al [1] and storing $\mathbf{P} = Z\mathbf{U}$ at each point.
- The pressure field was constructed by discretising Equation 1 along the radial direction for each position along the z axis and mapping the real part to give a snapshot of the field at $t = 0$.

5. Results

Results are presented in Figures 4 and 5 and show wavefronts expanding spherically for lower frequencies and directional propagation at higher frequencies. The theoretical results based on the multimodal theory are here compared to the experimental data measured using an array of 1/4" Roga RG-50 microphones microphones in the anechoic chamber of at the Institute of Musical Acoustics in the University of Music and Performing Arts of Vienna. The experimental method will be the topic of future publications. Results were normalised so that the real value of the pressure $z = 0, r = 0$ was one and contour lines are placed at spacings of 0.1 of that amplitude. The experimental and theoretical results show a good level of agreement, with the pressure wavefronts meeting the $z = 0$ plane at similar angles (showing an improvement with respect to using a hard walled expansion at $z = 0$, as this would imply pressure contours meeting the wall at 90 degrees). It is also possible to plot the theoretical radiated pressure field in the external pipe on the negative z side although this is not shown explicitly in this paper.

6. Acknowledgements

Thanks to Jean Kergomard for suggesting combining radiation from a source in an infinite baffle and a two sided (dipole) source in free space. Thanks also to Vasileios Chatziioannou and others at the Institute of Musical Acoustics in Vienna. The research leading to these results has received funding from the People Programme (Marie Curie Actions) of the European Unions Seventh Framework Programme FP7/2007-2013/ under REA grant agreement No. 605867 supporting the BATWOMAN ITN Project.

REFERENCES

1. Pagneux, V., Amir, N. and Kergomard, J. A study of wave propagation in varying cross-section waveguides by modal decomposition. part 1. theory and validation, *J. Acoust. Soc. Am.*, **100** (4), 2034–2048, (1996).

2. Amir, N., Pagneux, V. and Kergomard, J. A study of wave propagation in varying cross-section waveguides by modal decomposition. part 2. results, *J. Acoust. Soc. Am.*, **101** (5), 2504–2517, (1997).

3. Kemp, J., *Theoretical and experimental study of wave propagation in brass musical instruments*, Ph.D. thesis, University of Edinburgh, UK, `http://www.kempacoustics.com/thesis`, (2002).

4. Bruneau, A., Bruneau, M., Herzog, P. and Kergomard, J. Boundary layer attenuation of higher order modes in waveguides, *Journal of sound and vibration*, **119** (1), 15–27, (1987).

5. Mellow, T. J. and Kärkkäinen, L. M. On the sound field of a circular membrane in free space and an infinite baffle, *J. Acoust. Soc. Am.*, **120**, 2460–2477, (2006).

6. Mellow, T. On the sound field of a resilient disk in free space, *The Journal of the Acoustical Society of America*, **123** (4), 1880–1891, (2008).

7. Mellow, T. J. and Kärkkäinen, L. M. On the sound field of an oscillating disk in a finite open and closed circular baffle, *J. Acoust. Soc. Am.*, **118**, 1311–1325, (2005).

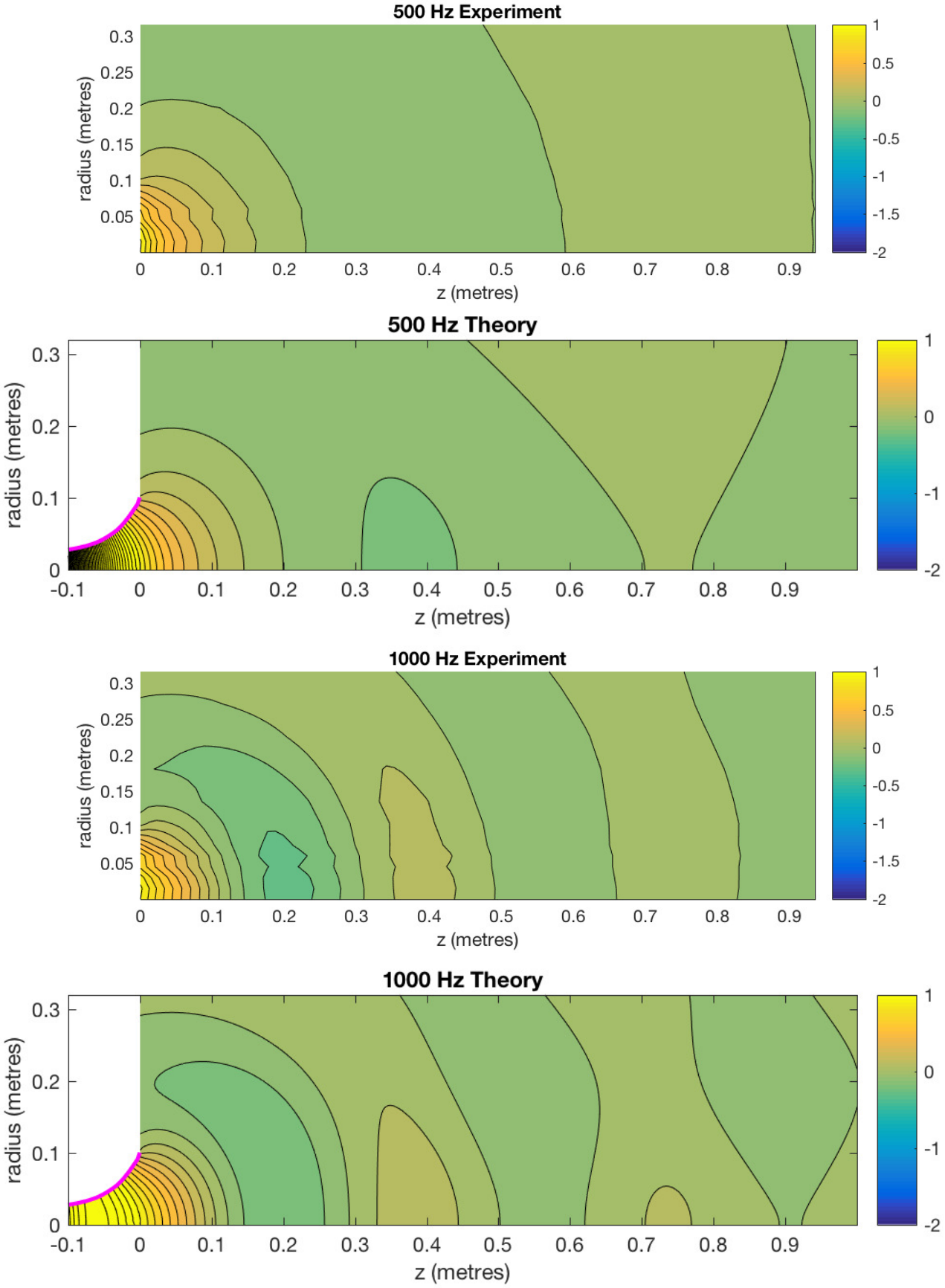

Figure 4: Real part of the normalised experimental and theoretical pressure fields for a Bach 36 Stradivarius series trombone. Theoretical results are for the trombone radiating into an external, infinite length, 6m radius cylinder with 800 modes used in the external cylinder and 16 modes inside the trombone bore. Experimental results were based on microphone array measurements in an anechoic chamber.

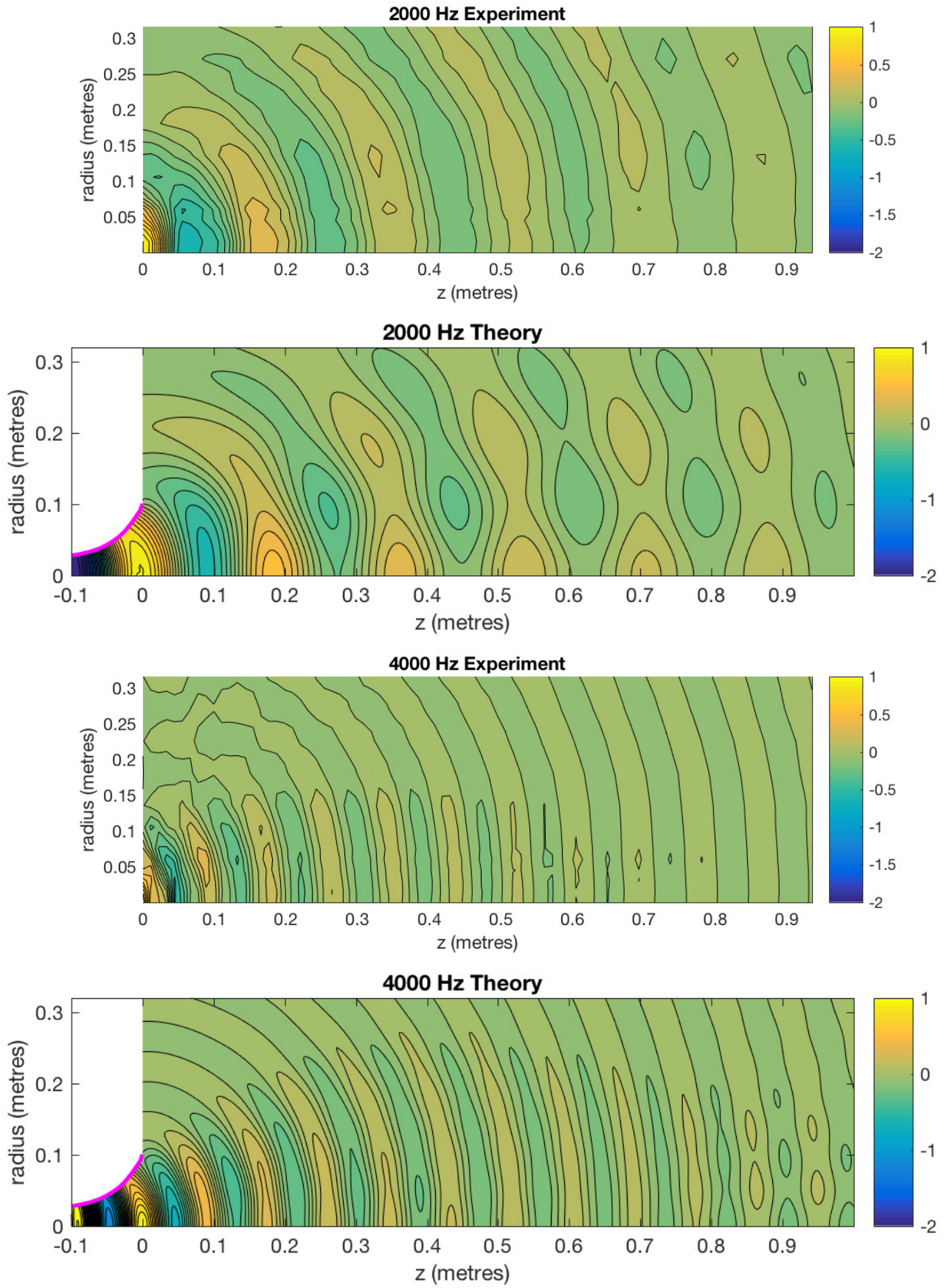

Figure 5: Real part of the normalised experimental and theoretical pressure fields for a Bach 36 Stradivarius series trombone. Theoretical results are for the trombone radiating into an external, infinite length, 6m radius cylinder with 800 modes used in the external cylinder and 16 modes inside the trombone bore. Experimental results were based on microphone array measurements in an anechoic chamber.